Ore Geology Reviews 94 (2018) 212–224

Contents lists available at ScienceDirect

Ore Geology Reviews

journal homepage: www.elsevier.com/locate/oregeorev

Geological and geochronological constraints on the formation of the Jurassic Maozaishan Sn deposit, Dayishan orefield, South China

Hairui Sun[a,b], Zheng Zhao[c,*], Guangsheng Yan[d], Zhicheng Lü[a,*], Zhilong Huang[e], Xiaofei Yu[a]

[a] Development and Research Center, China Geological Survey, Beijing 100037, China
[b] China University of Geosciences, Beijing 100083, China
[c] MLR Key Laboratory of Metallogeny and Mineral Assessment, Institute of Mineral Resources, Chinese Academy of Geological Sciences, Beijing 100037, China
[d] China Geological Survey, Beijing 100037, China
[e] State Key Laboratory of Ore Deposit Geochemistry, Institute of Geochemistry, Chinese Academy of Sciences, Guiyang 550005, China

ARTICLE INFO

Keywords:
Cassiterite
Geochronology
Dayishan orefield
Nanling Range
South China

ABSTRACT

The Dayishan orefield in the central Nanling belt is one of the most important Sn districts in South China. Within this district, there are more than seven medium-to-large Sn, Sn-Cu and Pb-Zn-Sn deposits. The mineralization is associated with altered granites and greisen-quartz veins, both of which occur in the inner part of the Dayishan granite batholith. Cassiterite is the principal ore mineral, accompanied by subordinate molybdenite. Cassiterite separates from altered and mineralized granite and greisen-quartz veins have concordia ages of 156.5 ± 2.8 Ma (MSWD = 3.1) and 158.0 ± 1.8 Ma (MSWD = 1.4), respectively. Molybdenite separates from molybdenite-quartz veins that crosscut the greisen alteration have a Re-Os isochron age of 157.9 ± 7.7 Ma (MSWD = 26), whereas zircon separates from the porphyry monzogranite have a U-Pb age of 156.3 ± 1.2 Ma. These ages are identical within the analytical error and, together with the field relationships, provide tight constraints on the Sn mineralization at around 156 Ma. Rhenium contents of the molybdenite suggests that the ore-forming materials were derived from a crustal source, whereas S and Pb isotopic data point to mixed sources. We suggest that the Maozaishan deposit was formed by intrusion of the related pluton, and occurred in the Late Jurassic during a period of lithospheric thinning and crustal extension of the South China Block.

1. Introduction

South China has been recognized as the most important W-Sn metallogenic region of the world (Liu et al., 2017). In the past decade, numerous geochronological studies have shown that the W-Sn polymetallic mineralization and related granitic magmatism in the Nanling Range have variable ages ranging from Late Triassic to Late Cretaceous, with most falling within a narrow range of 160–150 Ma (Mao et al., 2007; Yuan et al., 2015; Hu et al., 2017; Zhao et al., 2017) (Fig. 1a and b). Although the age of these deposits is well established, the precise genetic relationships between the ore-bearing granites and W-Sn deposits are still unclear because most metallogenic ages were obtained indirectly by a variety of techniques (Mao et al., 2007). Fortunately, cassiterite, which as main ore phase occurs in most Sn deposits, is ideal for direct dating of Sn-dominated, polymetallic mineralization. Numerous investigators have evaluated the cassiterite U-Pb isotope system as a geochronometer and demonstrated its reliability (Deng et al., 2017; Li et al., 2016; Yan et al., 2016; Yuan et al., 2008, 2011; Zhang et al., 2015).

In the Dayishan orefield, located at the central part of the Nanling Range, numerous alluvial Sn deposits have a proven reserve of 270,000 t of Sn, 78,000 t of Cu, 27,500 t of Pb + Zn and 483,686 t of B_2O_3 (Zeng, 2013). Recent exploration has revealed numerous large- to medium-sized Sn deposits stretching from the northwest to the southeast across the Dayishan batholith (Fig. 2). However, most of these deposits have not been exploited because of ecological concerns. Many geological studies of the Dayishan orefield, including basic geology, have already been carried out. Several more detailed investigations include a fluid inclusion study (Wu et al., 2008), an examination of stable isotopes (Zeng, 2013) and extensive age dating (Liu et al., 2006; Zhang et al., 2014). These studies have shown that the Sn-dominated, polymetallic deposits in this orefield formed at ca. 160 Ma and are genetically related to the associated late Jurassic granites. They have enhanced our understanding of the mineralization in the region, however, a well-constrained genetic model is still lacking because of a shortage of precise age data on the Sn mineralization, uncertainty on the source of the ore-forming materials and the nature of the geological environment.

* Corresponding authors at: No. 26, Baiwanzhuang Street, Xicheng District, Beijing 100037, China (Z. Zhao). Development and Research Center, China Geological Survey, No. 45 Fuwai Street, Xicheng District, Beijing 100037, China (Z. Lü).
E-mail addresses: kevin8572@hotmail.com (Z. Zhao), zhichenglv@163.com (Z. Lü).

https://doi.org/10.1016/j.oregeorev.2018.01.033
Received 26 October 2017; Received in revised form 29 January 2018; Accepted 30 January 2018
Available online 01 February 2018
0169-1368/

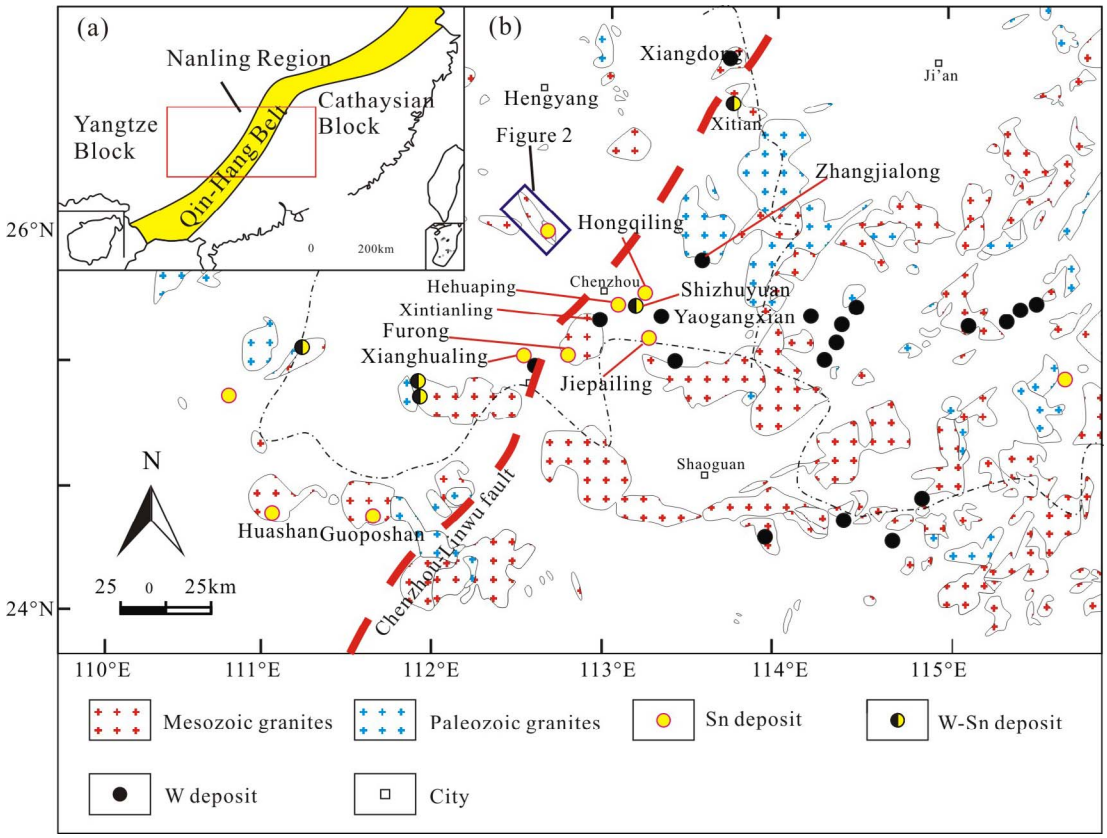

Fig. 1. (a) Sketch map showing the location of the Qin-Hang Belt of Mesozoic intrusive rocks in the South China (Modified after Mao et al., 2007, 2011); (b) simplified geological map of the Nanling Range showing the distribution of granitoids (Modified after Chen et al., 2014).

In the Maozaishan Sn deposit, there are two main types of mineralization, namely altered granite and greisen-quartz vein types. In this study, we summarized the existing isotopic and elemental data for W-Sn mineralization in the Nanling Range and obtained new cassiterite U-Pb, zircon U-Pb and molybdenite Re-Os ages, which enable us to directly constrain the age of the mineralization. We use these data to discuss the nature of the ore-forming materials and the geodynamic setting of the Sn-W deposits in the Dayishan orefield and the Nanling Range.

2. Regional geology

South China was formed by the Neoproterozoic collision of the Yangtze and Cathaysia Blocks along the Jiangshan-Shaoxing Fault (Fig. 1a) (Zhao et al., 2011). The Yangtze Block consists of crystalline basement overlain by Neoproterozoic (Sinian) to Cenozoic sedimentary strata (Zhou et al., 2014), whereas the Cathaysia Block consists of Precambrian basement and Sinian to Mesozoic sedimentary cover (Yu et al., 2005). Extensive magmatism in the Mesozoic produced widespread granitoid intrusions in South China (Li et al., 2009a; Ji et al., 2017). Spatially, these granitoid plutons are fault-controlled (Peng et al., 2006) and the Jurassic to Cretaceous magmatism is considered to be genetically related to the metallic mineralization in the Cathaysia Block (Hsieh et al., 2008) (Fig. 1b).

The Nanling Range, which has an area of ~200,000 km^2, is one of the 19 most important metallogenic belts in China (Chen et al., 2014). It consists of strongly folded and metamorphosed, Neoproterozoic-Ordovician flysch and volcanic basement overlain by Late Devonian to Early Triassic sedimentary rocks (Wang and Shu, 2012). Rift basins and granitoid intrusions are widespread in the region. The granitoid plutons formed by multiple cycles of tectono-magmatism, and are mostly directly associated with the W-Sn-rare metal mineralization (Zhang et al., 2015).

Previous studies of these plutons have shown that there is a NE-trending magmatic zone, referred to as the Qin-Hang belt or Shi-Hang zone, in which the magmatic rocks have high $\varepsilon_{Nd}(t)$ values and low T_{DM} ages (Gilder et al., 1996). The Qin-Hang zone is thought to have originated from mantle upwelling along a "paleo-rift" (Gilder et al., 1996; Tang et al., 2017). Abundant mafic microgranular enclaves (MMEs) in the granites are indicative of crust-mantle mixing (Zhu et al., 2008). Accompanying these granites are large Sn and W deposits, including the Furong and Hehuaping Sn deposits and the Shizhuyuan W-Sn-Bi-Mo deposit, amongst others. Most of the Sn and W deposits in this belt formed during the Late Jurassic to Early Cretaceous, except for the Late Triassic Qingshan W-Sn deposit (Zhao et al., 2018) and the Late Cretaceous Jiepailing Sn deposit (Chen et al., 2014; Peng et al., 2008; Yuan et al., 2015).

3. Ore deposit geology

The Dayishan orefield, central Qin-Hang belt, is located in southern Hunan Province. In this area, Sinian and Ordovician strata are mainly distributed south of the Dayishan granite batholith, and consist of weakly metamorphosed, clastic rocks with minor carbonates. These strata have been intruded by Mesozoic granitoid plutons (Fig. 2). Devonian, Carboniferous and Permian strata are widespread in the area and consist mainly of carbonates with minor clastic rocks. The Dayishan granite batholith, which appears to have been controlled by a NW-trending fault, has an elliptical shape with a total outcrop area of 280 km^2 (Fig. 2). It is a polyphase body with three components, from SE to NW, referred to as the Guankou, Tangshipu and Nibantian granites. These magmatic phases consist mostly of coarse-, medium- and medium- to fine-grained porphyritic granites (Wu et al., 2005; Zhou et al., 2005) with SiO_2 contents in the range of 67.0–73.12 wt%. The granites are strongly peraluminous, calc-alkaline rocks, with Al_2O_3

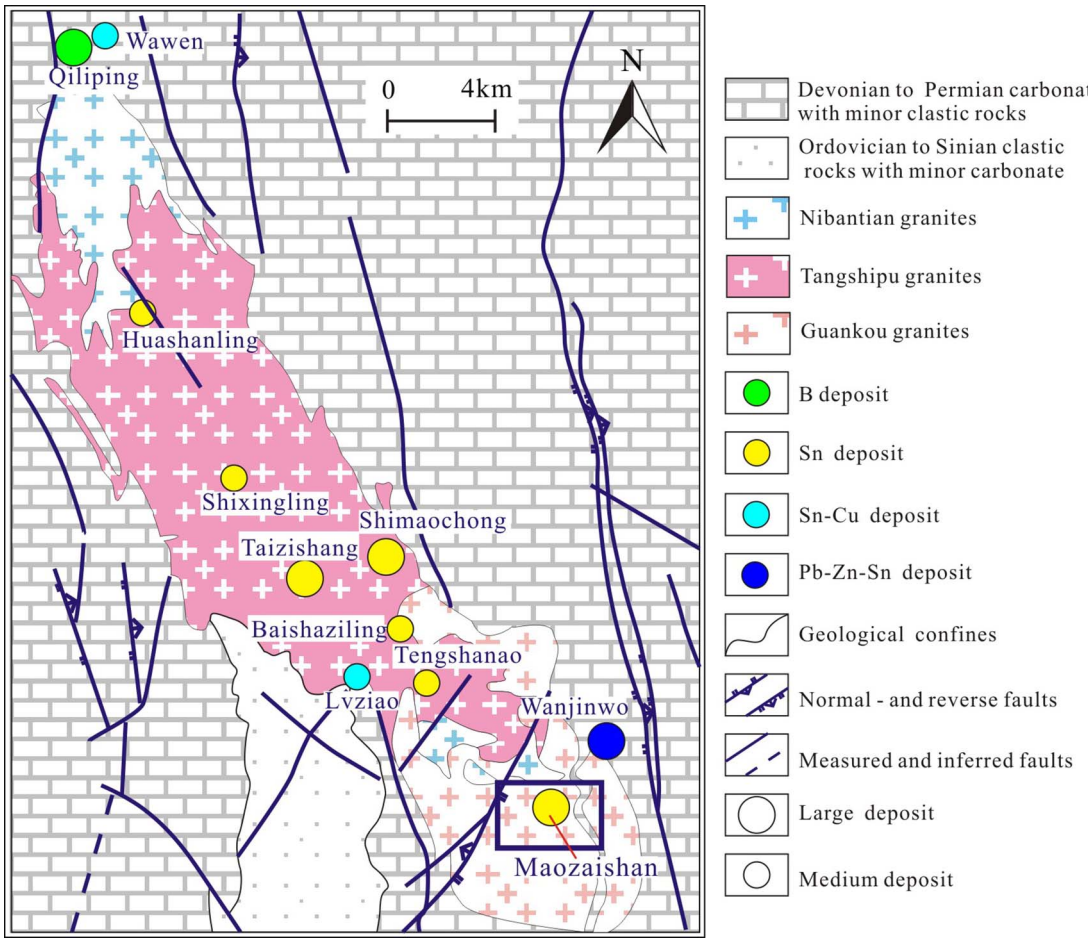

Fig. 2. Simplified regional geological map of the Dayishan Sn-dominated, polymetallic orefield (Modified after Zeng, 2013).

contents of 11.81–15.13 wt%, $K_2O + Na_2O$ contents of 6.54–8.82 wt%, K/Na ratios > 1.3 and A/CNK ratios > 1.1 (Zeng, 2013). These rocks are generally similar to A-type granites (Kong et al., 2014), with 10,000 Ga/Al values of 3.47–4.00. K-Ar ages of biotite and muscovite and U-Pb zircon ages, suggest that the granites were intruded between 223 Ma and 140 Ma (Wu and Peng, 2000).

In the Dayishan orefield, there are more than seven Sn deposits, including from NW to SE, the Wawen Sn-Cu deposit, the Huashanling, Shixingling, Taizishang, Shimaochong, Baishaziling, Tengshanao and Maozaishan Sn deposits and some B, Pb-Zn-Sn and As deposits. Of these, the altered granite and greisen-quartz vein-types of mineralization are most important and are concentrated in the interior of the batholith. The deposits are usually oval in shape and occur in clusters. In the interior of the Maozaishan area, faults strike E-W, NW and N-S; the E-W and N-S structures are the best developed and appear to have controlled much of the Sn mineralization. The ore minerals consist mainly of cassiterite, arsenopyrite, pyrite, chalcopyrite, wolframite and tetrahedrite with minor molybdenite and bismuthinite. Gangue minerals are predominately quartz, mica and tourmaline with minor fluorite and topaz. Hydrothermal alteration occurs as greisenization, silicification, skarnization, sericitization and chloritization.

The medium-sized Maozaishan deposit is located in the extreme SE of the Dayishan granite batholith and contains important greisen-quartz vein- and altered granite-type mineralization. The Sn mineralization is hosted in the Guankou granites at the surface. The extensive Guankou phase consists chiefly of porphyritic, A-type granite with minor occurrences of the Nibantian granites in the northern part of the area (Fig. 3a). More than 20 individual Sn ore veins have been discovered in this deposit. These veins are parallel to each other, mostly dip steeply (> 70°) and display predominantly NW and minor E–W trends. Individual vein is up to 900 m long, 0.5 m wide and may extend to > 100 m below the surface (Fig. 3b). They typically occur in en echelon patterns and clusters (Fig. 3a and b), with cassiterite, arsenopyrite and pyrite mineralization accompanied by minor chalcopyrite and sphalerite, as well as the typical gangue minerals as described above. Ore textures and mineral assemblages, as well as crosscutting vein relationships, indicate the following general paragenetic sequence: (1) early greisen alteration followed by (2) Sn greisen-quartz veining or ore formation (Fig. 4a–d and g). Molybdenite in the quartz veins postdates the greisen alteration but was earlier than the Sn greisen-quartz vein stage (Fig. 4c, d and h).

The Sn mineralization associated with altered granite in the Maozaishan deposit is locally distributed at depth and is characterized by a layer of pegmatite above the ore body. The ore textures and associations are relatively simple and the mineralization is predominantly disseminated (Fig. 4e and f). Ore minerals include cassiterite and minor arsenopyrite, wolframite, chalcopyrite and sphalerite, with quartz, K-feldspar, albite, mica and tourmaline as gangue minerals. Tourmaline is mostly randomly distributed but may locally form clusters (Fig. 4e). Greisenization is the main alteration type and is closely related to cassiterite deposition.

4. Sampling and analytical methods

4.1. Zircon U-Pb dating

Sample MC29-10 consists of porphyritic, monzonitic granite collected from the related Sn mineralized granite in the Maozaishan

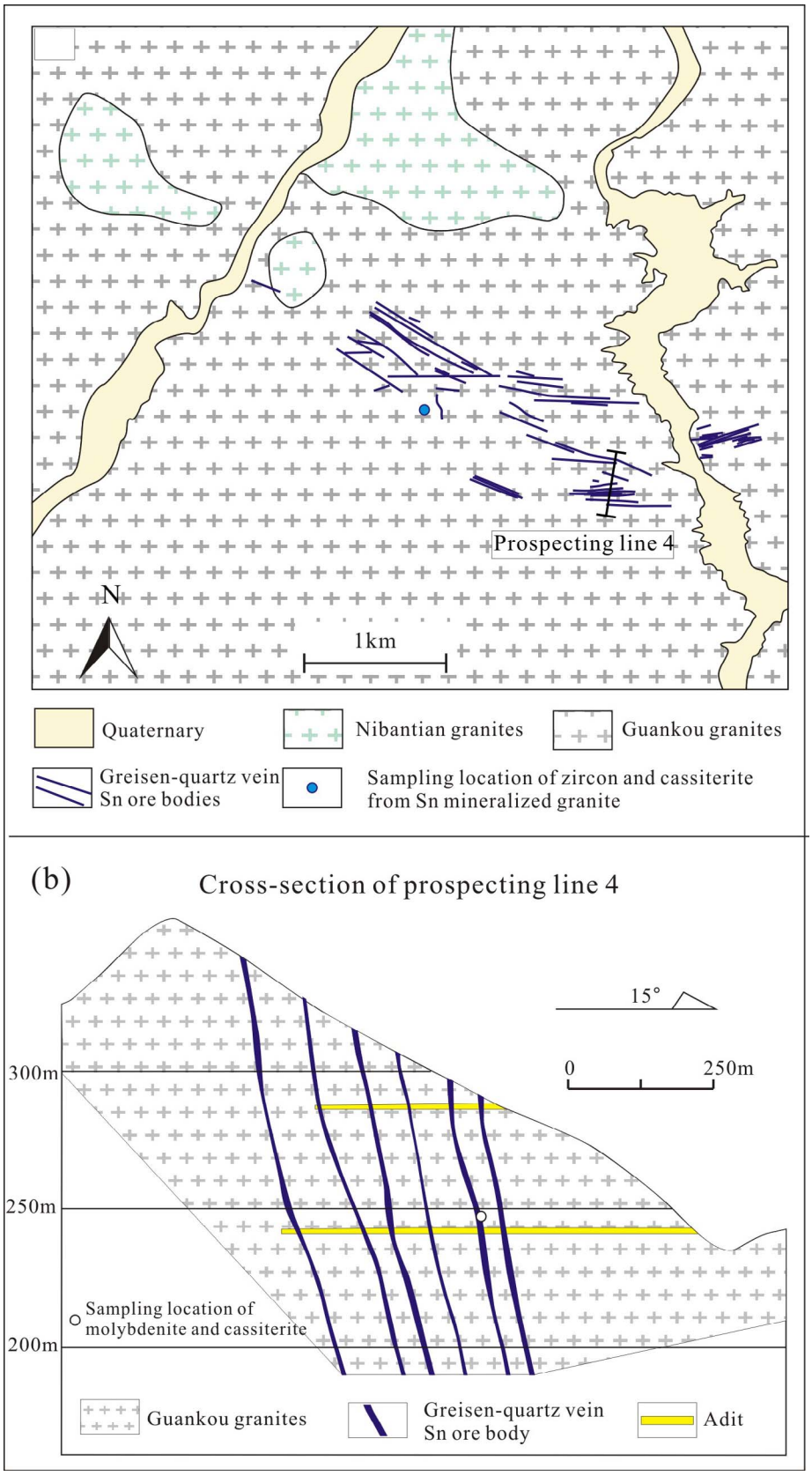

Fig. 3. (a) Simplified geological map and (b) cross–section of prospecting line 4 of the Maozaishan Sn deposit.

deposit (Fig. 4e). Zircon grains were separated using standard magnetic and heavy liquid techniques, followed by handpicking under a binocular microscope. High-quality grains were mounted in epoxy resin and polished to approximately half their thickness. Cathodoluminescence (CL) images were used to investigate the zircon textures and to choose target sites for U–Pb isotopic dating.

The U-Pb geochronology of the zircons was determined using laser ablation, inductively coupled mass spectrometry (LA-ICP-MS) at the

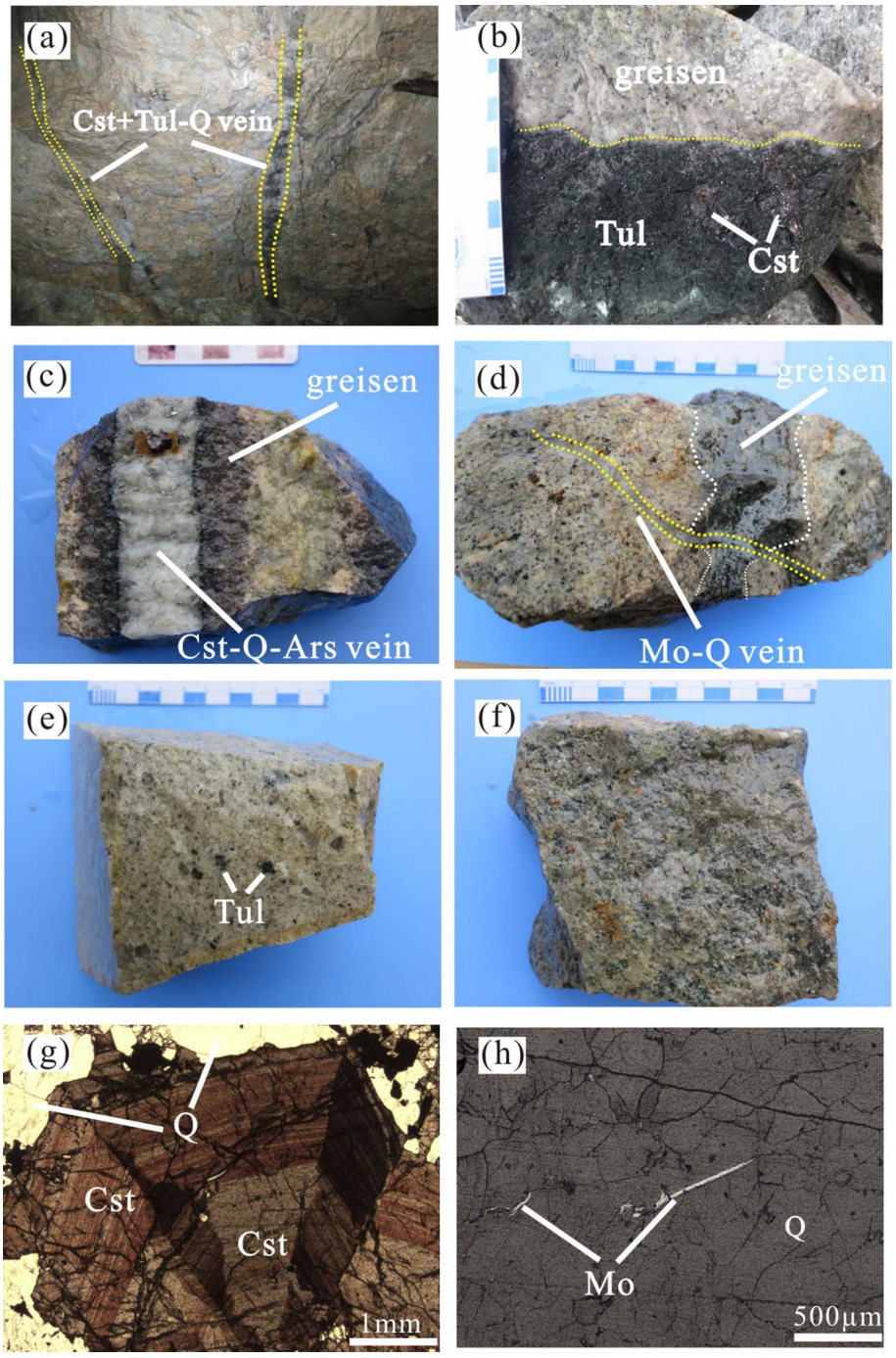

Fig. 4. Photographs of significant features in the Maozaishan Sn deposit. (a) Cassiterite + quartz + tourmaline vein cutting pegmatite; (b) cassiterite + quartz + tourmaline vein cutting greisen; (c) Zones of greisen mineralization separate the vein from the altered granite, which contains abundant chlorite; (d) quartz + molybdenite vein cutting a zone of early greisen-quartz vein-type Sn mineralization; (e) unaltered ore-forming, porphyritic, monzonitic granite containing small tourmaline clusters; (f) Sn-bearing, greisen, porphyritic, monzonitic granite; (g) photomicrograph of cassiterite with clear concentric, oscillatory zoning in a quartz vein; (h) photomicrograph of molybdenite in quartz vein. Abbreviations: Cst = Cassiterite; Tul = tourmaline; Q = Quartz; Mo = Molybdenite.

State Key Laboratory of Geological Processes and Mineral Resources, China University of Geosciences, Wuhan. The analytical system consists of a GeoLasPro laser ablation system (Lamda Physik, Gottingen, Germany) and an Agilent 7700x ICP-MS. A 193 nm ArF excimer laser beam was homogenized by a set of beam delivery systems, and the beam was focused on each zircon surface with a fluence of 10 J/cm^2. A spot diameter of 44 μm at 3 Hz was employed. Helium was used as the carrier gas to transport aerosols to the ICP-MS.

Zircon 91,500 was used as an external standard to correct instrumental mass discrimination and elemental fractionation. Standard zircons GJ-1 and Plešovice were used for quality control. The Pb abundance in zircon was externally calibrated against NIST SRM 610 using Si as the internal standard. Zirconium was used as an internal standard for the other trace elements (Liu et al., 2010a). Raw data calculations were performed offline using ICPMSDataCal software (Liu et al., 2010a,b).

4.2. Cassiterite U-Pb dating

Two cassiterite samples (HW-25 and MC29-16) were collected from the Maizaishan deposit for U-Pb dating; one from a greisen-quartz vein showing Sn mineralization and the other from the Sn-bearing greisen in the monzonitic granite (Fig. 4c and f, respectively). The samples were crushed to 40–60 mesh and cassiterite grains were separated using standard heavy liquid and magnetic techniques. Grains were then handpicked under a binocular microscope, and mounted with an in-house cassiterite standard (Lbiao) in an epoxy resin disc and polished.

Internal textures were examined under the microscope to identify

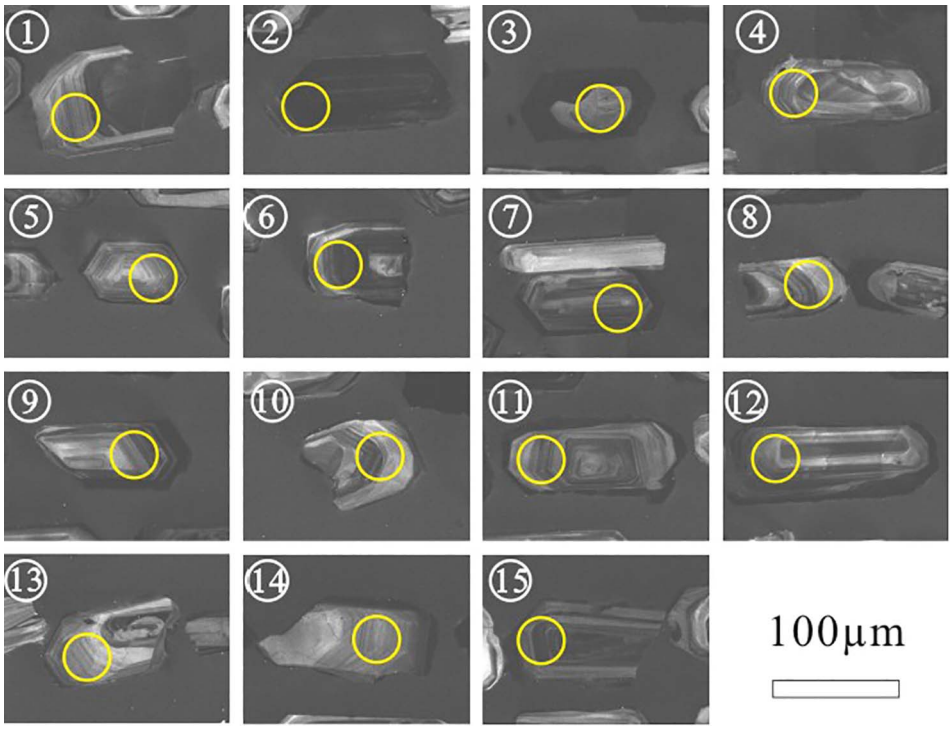

Fig. 5. Cathodoluminescence (CL) images of zircons from the unaltered, porphyritic monzonitic granite of the Maozaishan Sn deposit. Yellow circle show analytical spots.

inclusion-free grains for U-Pb analyses. In situ U-Pb dating was performed at the Tianjin Institute of Geology and Mineral Resources using a Neptune MC-ICP-MS (Thermo Fisher Scientific Inc., Waltham, Massachusetts, USA) coupled with a 193 nm UP193FX ArF excimer laser ablation system (Electro Scientific Industries, Inc., Portland, Oregon, USA). The MC-ICP-MS instrument was equipped with one axial Faraday cup, eight off-axis Faraday cups and four ion counters. The laser system was operated with an ~5 ns pulse. Using reflected and transmitted light images, the laser was focused to produce an ablation pit with a 35–50 μm diameter at a laser pulse rate of 8–10 Hz and energy density of 13–14 J/cm^2. To correct for matrix effects, the Lbiao cassiterite was used as an in-house standard (U-Pb age of 158.2 ± 0.4 Ma by ID-TIMS, Yuan et al., 2011). For each analysis of an unknown, one external standard measurement was also made. Each analysis incorporated a background acquisition time of 20 s followed by 40 s of data acquisition. Additional details of the instrument parameters and conditions are described in Yuan et al. (2011). The $^{207}Pb/^{206}Pb$, $^{206}Pb/^{238}U$ and $^{207}Pb/^{235}U$ ratios were corrected using the cassiterite external standard, and calculated ages were determined using Isoplot 4.0 (Berkeley Geochronology Center, Berkeley, California, USA).

4.3. Molybdenite Re-Os dating

Samples for Re-Os analysis were collected from a molybdenite-quartz vein, which crosscuts the Sn greisen-quartz vein mineralization (Fig. 4d and h). These late molybdenite-quartz veins help to constrain the age of the greisen-quartz vein mineralization. Molybdenite grains were selected using an optical microscope and magnetic methods. Fresh, non-oxidized molybdenite separates, 0.2–0.5 mm in diameter, were handpicked using a binocular microscope.

The Re-Os isotope analyses were carried out at the National Research Center of Geoanalysis, Chinese Academy of Geological Sciences, Beijing. The instrument used was a TJA X-series ICP-MS (Thermo Fisher Scientific Inc., Waltham, Massachusetts, USA). Details of the analytical procedure are described in Shirey and Walker (1995) and Du et al. (2004). The molybdenite standard GBW04436 (JDC) with a certified age of 139.6 ± 3.8 Ma (Du et al., 2004) was used in this study and gave model ages within error of the certified age (138.2 ± 2.0 Ma and 139.6 ± 1.9 Ma). Blanks used in this study contained 93.9 pg and 35.6 pg of Re, and 14 pg and 4 pg of Os. Model ages were calculated using Eq. (1):

$$t = [\ln(1 + {}^{187}Os/{}^{187}Re)]/\lambda \quad (1)$$

where λ is the decay constant of ^{187}Re ($1.666 \times 10^{-11}/yr^{-1}$) (Smoliar et al., 1996).

5. Results

5.1. Zircon U-Pb ages

Fifteen zircon grains from sample MC29-10 were selected for LA-ICP-MS analysis. The selected zircons are light pink to colorless and transparent, mostly euhedral and 100–300 μm in length, with length-to-width ratios of 2:1 to 3:1. Concentric oscillatory zoning is evident from CL images (Fig. 5), a feature that is typical of magmatic zircon. No inherited cores were found in the samples.

The average age of zircons in the sample was calculated based on the weighted mean of the common Pb-corrected $^{206}Pb/^{238}U$ ages at 95% confidence level. The results are interpreted to represent the emplacement age of the granite.

The results of zircon U-Pb dating for all grains are given in Table 1. The U and Th contents in the zircons vary significantly, with values in the 79–2724 ppm and 50–688 ppm range, respectively, yielding Th/U ratios of 0.10–0.62. The $^{206}Pb/^{238}U$ ages of 15 zircon grains from sample MC29-10 range from 155.7 to 156.7 Ma, yielding a weighted $^{206}Pb/^{238}U$ age of 156.3 ± 1.2 Ma (Fig. 6). The results indicate that the porphyritic monzonitic granite was emplaced in the late Jurassic.

5.2. Cassiterite U-Pb ages

A total of 45 cassiterite separates were analyzed from sample MC29-16 (altered, porphyritic monzonitic granite). The cassiterite grains are yellow to brown and some contain inclusions and cracks, which were avoided during U-Pb isotopic analysis. The analytical results are presented in Table 2.

The isotopic ratios show large variations, with $^{238}U/^{207}Pb$ in the

Table 1
Zircon U–Pb isotope composition for porphyry monzonitic granite.

Sample spots	Th	U	Th/U	$^{207}Pb/^{206}Pb$		$^{207}Pb/^{235}U$		$^{206}Pb/^{238}U$		$^{207}Pb/^{206}Pb$		$^{207}Pb/^{235}U$		$^{206}Pb/^{238}U$		$^{208}Pb/^{232}Th$	
				Ratio	1σ	Ratio	1σ	Ratio	1σ	Age (Ma)	1σ	Age (Ma)	1σ	Age (Ma)	1σ	Age (Ma)	1σ
MC-29-10-1	277	2724	0.10	0.0494	0.0016	0.1661	0.0054	0.0245	0.0004	169	71.3	156	4.7	156	2.3	160	6.3
MC-29-10-2	688	1669	0.41	0.0502	0.0014	0.1702	0.0049	0.0245	0.0003	211	63.0	160	4.2	156	1.6	155	3.4
MC-29-10-3	170	306	0.55	0.0508	0.0015	0.1714	0.0053	0.0244	0.0002	232	68.5	161	4.6	156	1.6	151	3.5
MC-29-10-4	132	356	0.37	0.0486	0.0018	0.1648	0.0061	0.0246	0.0003	132	85.2	155	5.3	156	1.8	167	4.6
MC-29-10-5	515	1522	0.34	0.0453	0.0018	0.1523	0.0061	0.0245	0.0005	120	88.0	144	5.4	156	3.1	144	3.5
MC-29-10-6	300	933	0.32	0.0465	0.0011	0.1579	0.0037	0.0245	0.0002	33	46.3	149	3.3	156	1.5	160	3.1
MC-29-10-7	157	467	0.34	0.0490	0.0017	0.1651	0.0053	0.0245	0.0003	146	84.2	155	4.6	156	1.8	153	3.6
MC-29-10-8	98	186	0.53	0.0492	0.0019	0.1672	0.0068	0.0246	0.0003	167	95.4	157	5.9	157	2.1	160	4.0
MC-29-10-9	294	825	0.36	0.0484	0.0017	0.1637	0.0059	0.0246	0.0004	121	88.0	154	5.2	156	2.5	144	3.6
MC-29-10-10	292	1579	0.19	0.0438	0.0025	0.1498	0.0088	0.0246	0.0004	233	75.0	142	7.8	157	2.4	154	4.9
MC-29-10-11	93	201	0.46	0.0481	0.0013	0.1630	0.0050	0.0245	0.0004	106	66.7	153	4.3	156	2.2	147	4.0
MC-29-10-12	50	79	0.62	0.0518	0.0016	0.1764	0.0056	0.0246	0.0002	276	67.6	165	4.8	157	1.6	153	3.5
MC-29-10-13	118	262	0.45	0.0520	0.0026	0.1772	0.0096	0.0245	0.0004	283	114.8	166	8.3	156	2.3	151	4.2
MC-29-10-14	108	844	0.13	0.0502	0.0019	0.1703	0.0068	0.0246	0.0004	206	88.9	160	5.9	157	2.3	163	4.5
MC-29-10-15	159	465	0.34	0.0510	0.0012	0.1740	0.0042	0.0246	0.0003	243	53.7	163	3.7	157	1.6	176	3.7

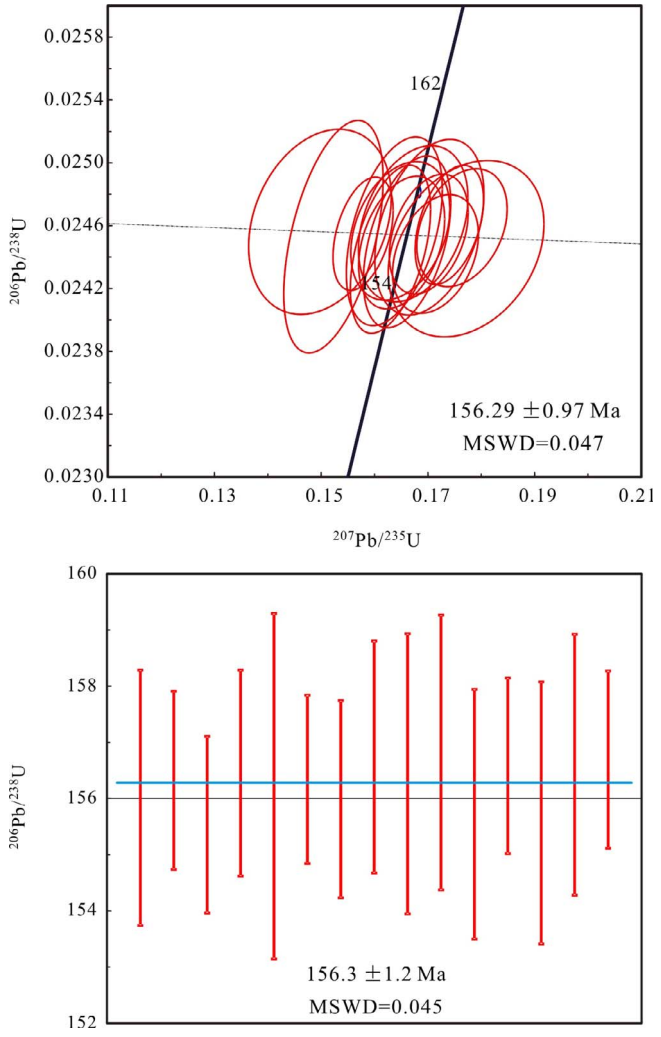

Fig. 6. LA–ICP–MS zircon U–Pb diagrams of granite from the Maozaishan Sn deposit, based on the analyses shown in Fig. 5.

7.5–670 range and $^{206}U/^{207}Pb$ in the 1.34–17.8 range. After correction for common Pb, the analyses yielded a $^{206}Pb/^{207}Pb$-$^{238}U/^{207}Pb$ isochron age of 153.5 ± 3.4 Ma (MSWD = 1.16) with an initial $^{206}Pb/^{207}Pb$ ratio of 1.253. In comparison, the Tera-Wasserburg concordia age of 156.5 ± 2.8 Ma (MSWD = 3.1) is slightly older, but is consistent within error. This concordia age represents the age of mineralization in the altered granite (Fig. 7a and b). This interpretation is consistent with the conclusion of Li et al. (2016) that the Tera-Wasserburg, U-Pb intercept age is far better than the previously used $^{206}Pb/^{207}Pb$ vs. $^{238}U/^{207}Pb$ "isochron" age for cassiterite.

Forty-three cassiterite grains were analyzed from sample HW-25, which is characterized by greisen-quartz vein-type mineralization. Ratios of $^{238}U/^{207}Pb$ and $^{206}U/^{207}Pb$ also show large variations with values in the range of 16.5–813 and 1.61–24.0, respectively. After correction for common Pb, the analyses yielded a $^{206}Pb/^{207}Pb$–$^{238}U/^{207}Pb$ isochron age of 157.7 ± 6.2 Ma (MSWD = 0.43) with an initial $^{206}Pb/^{207}Pb$ ratio of 1.174. By comparison, the Tera-Wasserburg concordia age of 158.0 ± 1.8 Ma (MSWD = 1.4) is older but is consistent within error. It is likely that the concordia age represents the age of the greisen-quartz vein-type mineralization (Fig. 7c and d).

5.3. Molybdenite Re-Os ages

Five molybdenite separates from molybdenite-quartz veins in the Maozaishan deposit were analyzed for Re and Os isotopes (Table 3). The Re and ^{187}Os contents of the molybdenite separates are in the range of 94.94–5570 ppb and 0.1681–8.977 ppb, respectively. The data produce a relatively well-constrained Re-Os model age of 153.7 ± 0.7 to 168.8 ± 0.8 Ma, with a weighted mean age of 161.0 ± 8.5 Ma (MSWD = 54). These samples yield an ^{187}Re-^{187}Os isochron age of 157.9 ± 7.7 Ma (MSWD = 26) which, within error, accords well with the weighted mean age (Fig. 8a and b).

6. Discussion

6.1. Timing of Sn mineralization

Very few studies on the mineralization age have been carried out for the Sn deposits in the Dayishan orefield. Zhang et al. (2014) reported an Rb-Sr isochron age of 160 ± 1 Ma for fluid inclusions in quartz of a cassiterite-quartz vein from the Baishaziling Sn deposit north of the Maozaishan deposit. However, precisely constraining the Sn mineralization age is not straightforward because the fluid inclusions in the quartz veins are complex and rarely contain a single fluid stage.

Direct dating of cassiterite U-Pb ages in this study provide constraints on the mineralization age of the Maozaishan Sn deposit. In general, most primary Sn deposits are closely related, both temporally and spatially, to the emplacement of the associated granitic rocks (Lehmann, 1982). Thus, the emplacement ages of ore-related granites can be used to constrain the ages of Sn mineralization, as is shown for

Table 2
Cassiterite U–Pb isotope composition of Maozaishan tin deposit.

Sample spots	$^{238}U/^{207}Pb$	1σ	$^{206}Pb/^{207}Pb$	1σ	$^{238}U/^{206}Pb$	1σ
Altered granite tin mineralization						
MC29-16-1	90.03	19.13	3.88	19.83	25.82	6.15
MC29-16-2	59.76	7.98	2.76	6.75	23.26	3.93
MC29-16-3	308.24	5.11	8.81	4.75	37.07	2.00
MC29-16-4	173.81	14.76	5.58	9.12	34.79	4.01
MC29-16-5	204.88	15.26	6.66	15.82	33.19	3.21
MC29-16-6	140.56	11.03	4.40	10.67	33.98	3.11
MC29-16-7	15.95	4.34	1.59	2.48	10.69	3.27
MC29-16-8	351.10	7.71	9.85	7.06	38.08	2.08
MC29-16-9	162.74	5.42	5.16	4.82	33.45	2.24
MC29-16-10	141.56	12.05	4.71	11.52	32.14	3.58
MC29-16-11	212.22	8.50	6.54	7.78	34.71	2.34
MC29-16-12	280.73	7.22	8.00	6.71	37.32	2.11
MC29-16-13	259.31	6.46	7.49	6.00	36.75	2.08
MC29-16-14	348.31	16.39	10.40	15.60	37.06	2.78
MC29-16-15	124.94	6.98	4.18	6.14	31.94	2.62
MC29-16-16	48.92	10.12	2.26	10.60	22.45	5.02
MC29-16-17	85.65	9.14	3.35	7.65	27.74	3.59
MC29-16-18	76.33	12.01	2.74	13.50	28.00	4.91
MC29-16-19	91.50	12.34	3.40	11.14	29.26	4.19
MC29-16-20	468.33	8.43	12.68	8.20	39.20	2.03
MC29-16-21	129.46	9.15	4.25	8.19	33.19	3.15
MC29-16-22	55.78	8.22	2.59	6.92	23.01	3.76
MC29-16-23	340.68	6.71	9.47	6.36	38.16	2.04
MC29-16-24	448.28	7.46	12.32	6.94	38.79	2.05
MC29-16-25	196.45	4.79	5.87	4.48	35.38	2.06
MC29-16-26	114.23	6.41	4.00	5.62	30.35	2.74
MC29-16-27	218.87	9.78	6.64	9.67	34.98	2.49
MC29-16-28	145.98	17.52	5.35	19.44	30.23	4.45
MC29-16-29	7.49	8.67	1.34	4.79	5.91	7.50
MC29-16-30	252.67	13.17	7.68	12.91	35.29	2.59
MC29-16-31	353.94	19.45	10.36	20.40	36.42	3.03
MC29-16-32	264.75	14.98	7.48	15.12	38.07	3.04
MC29-16-33	180.26	16.34	5.43	16.60	36.94	4.10
MC29-16-34	430.61	9.03	11.60	8.57	39.57	2.11
MC29-16-35	296.02	9.82	8.72	9.03	36.61	2.33
MC29-16-36	670.26	12.47	17.77	12.28	40.14	2.06
MC29-16-37	217.19	13.60	6.43	13.26	36.01	3.10
MC29-16-38	115.54	15.90	4.18	15.90	30.13	4.68
MC29-16-39	146.42	23.88	5.36	37.96	32.16	6.13
MC29-16-40	101.40	8.38	3.79	8.10	28.42	3.14
MC29-16-41	54.09	4.12	2.50	3.73	22.77	2.42
MC29-16-42	72.38	9.49	2.93	9.33	25.93	3.60
MC29-16-43	207.45	5.49	6.18	5.04	35.65	2.10
MC29-16-44	166.64	11.57	5.66	10.57	32.53	3.06
MC29-16-45	9.45	3.07	1.49	2.35	6.67	2.74
Greisen-quartz vein tin mineralization						
HW-25-1	277.97	33.04	8.20	35.21	37.13	4.77
HW-25-2	290.84	41.32	8.95	48.82	35.50	6.14
HW-25-3	256.44	28.04	8.06	31.84	35.28	5.03
HW-25-4	619.93	27.94	19.80	34.76	39.42	5.85
HW-25-5	210.56	18.73	5.91	18.79	37.80	3.88
HW-25-6	175.45	13.64	5.49	13.68	34.11	3.44
HW-25-7	417.41	15.08	11.34	14.73	39.21	2.66
HW-25-8	765.61	29.08	20.89	29.60	39.86	2.49
HW-25-9	511.38	28.94	14.36	30.03	38.83	2.94
HW-25-10	534.23	25.24	14.82	26.84	38.66	3.91
HW-25-11	523.75	7.92	14.21	7.83	39.60	1.99
HW-25-12	182.28	26.00	5.52	26.81	34.69	8.51
HW-25-13	274.26	16.86	8.08	16.39	37.62	3.27
HW-25-14	109.25	27.05	3.72	29.49	29.77	15.01
HW-25-15	287.40	13.35	8.20	13.26	37.90	3.03
HW-25-16	267.42	21.41	7.70	21.48	37.05	3.36
HW-25-17	417.08	38.65	11.63	41.26	38.57	4.37
HW-25-18	365.34	10.88	10.43	10.73	37.71	2.25
HW-25-19	59.94	11.77	2.45	13.34	25.16	5.43
HW-25-20	813.34	28.03	24.03	35.96	39.93	3.58
HW-25-21	503.13	11.14	13.59	11.18	39.81	2.18
HW-25-22	42.83	2.66	2.23	2.34	20.62	1.90
HW-25-23	633.16	11.45	17.00	11.22	40.15	1.98
HW-25-24	380.91	26.84	12.22	21.80	35.66	7.79
HW-25-25	161.97	11.34	5.32	11.06	32.73	2.82
HW-25-26	51.46	4.30	2.49	4.32	22.12	2.55
HW-25-27	472.85	25.27	13.51	25.37	37.92	2.75
HW-25-28	287.42	23.15	8.23	24.25	38.71	4.15
HW-25-29	249.96	8.67	7.54	8.20	35.75	2.20
HW-25-30	133.44	24.23	4.59	23.51	31.84	6.38
HW-25-31	662.05	12.58	17.82	12.53	40.04	2.04
HW-25-32	665.27	15.42	17.65	15.24	40.69	2.09
HW-25-33	16.44	3.67	1.61	3.93	10.91	2.73
HW-25-34	602.13	26.84	16.33	27.24	40.10	2.55
HW-25-35	190.72	34.73	6.29	39.28	33.87	7.38
HW-25-36	221.95	16.27	6.90	15.62	35.14	3.27
HW-25-37	556.77	10.94	15.18	10.82	39.48	2.04
HW-25-38	582.52	28.80	16.88	25.58	38.80	4.71
HW-25-39	722.18	24.18	21.83	28.65	39.97	3.49
HW-25-40	211.72	18.21	6.43	16.92	36.14	3.73
HW-25-41	313.81	24.27	10.12	25.74	36.60	6.64
HW-25-42	93.53	5.19	3.41	5.22	29.36	2.36
HW-25-43	407.58	24.32	11.46	25.12	38.63	2.70

the Sn deposit. In fact, the zircon grains from the ore-related granite at Maozaishan yielded a $^{206}Pb/^{238}U$ weighted age of 156.3 ± 1.2 Ma, which is likely the age of the altered granite-type mineralization. Cassiterite, which is typically the dominant ore mineral in Sn deposits, has a measurable U content and is generally not easily affected by late hydrothermal events. Thus, cassiterite U-Pb ages may directly constrain the timing of Sn mineralization, which is why this technique has attracted considerable interest in recent years (Deng et al., 2017; Li et al., 2016; Yan et al., 2016; Yuan et al., 2008, 2011; Zhang et al., 2015). The in situ U-Pb dating of cassiterite reported in this study from the greisen-quartz vein and altered porphyry monzogranite mineralization yielded $^{238}U/^{206}Pb$-$^{207}U/^{206}Pb$ Tera-Wasserburg concordia ages of 158.0 ± 1.8 Ma and 156.5 ± 2.8 Ma, respectively. Recently, Li et al. (2016) found that the Tera–Wasserburg U–Pb intercept age is far better than the previously used $^{206}Pb/^{207}Pb$ versus $^{238}U/^{207}Pb$ "isochron" age because the latter weights data points with low proportions of common Pb more heavily, thus introducing larger errors. In addition, five molybdenite samples were obtained from quartz veins that crosscut the greisen alteration and these yielded a Re-Os isochron age of 157.9 ± 7.7 Ma. Thus, the concordia ages of cassiterite reported in this study are considered more reliable because the errors are smaller and the results closely match the Re-Os and zircon U-Pb ages. Collectively, isotopic data for the Maozaishan deposit suggest that the two types of Sn mineralization took place at ca. 158–156 Ma.

Previous work in the Nanling Range has shown that W-Sn metallogenesis was active during the Caledonian, Indosinian and Yanshanian orogenies (Chen et al., 2014). Although some Triassic and Cretaceous mineralization has been reported, large-scale W-Sn polymetallic mineralization in the Nanling Range typically took place within a 160–150 Ma interval (Hu et al., 2017; Mao et al., 2007; Peng et al., 2008), which is consistent with the ages of Sn-dominated polymetallic mineralization in the Dayishan orefield and the results of this study (Mao et al., 2007; Peng et al., 2006).

6.2. Source of the ore-forming materials

During analysis of the Re-Os isotopic composition of the molybdenite grains from the Maozaishan deposit, the Re contents were also obtained. Mao et al. (1999) have suggested that the Re content of molybdenite can indicate its source; crustal ($n \times 10^{-6}$), crust-mantle ($n \times 10^{-5}$) or mantle ($n \times 10^{-4}$) compositions. Molybdenite samples from the Maozaishan deposit have Re contents in the 95.0–5570 ppb range, with most values exceeding 4000 ppb (Fig. 9). These values compare favorably with those from other Sn and W deposits along the Qin-Hang belt. In addition, sulfur isotope data from the Sn deposits of the Dayishan orefield mostly fall in the 1–3‰ range (Fig. 10) and lead isotope data display mixed signatures (Fig. 11), similar to isotopic

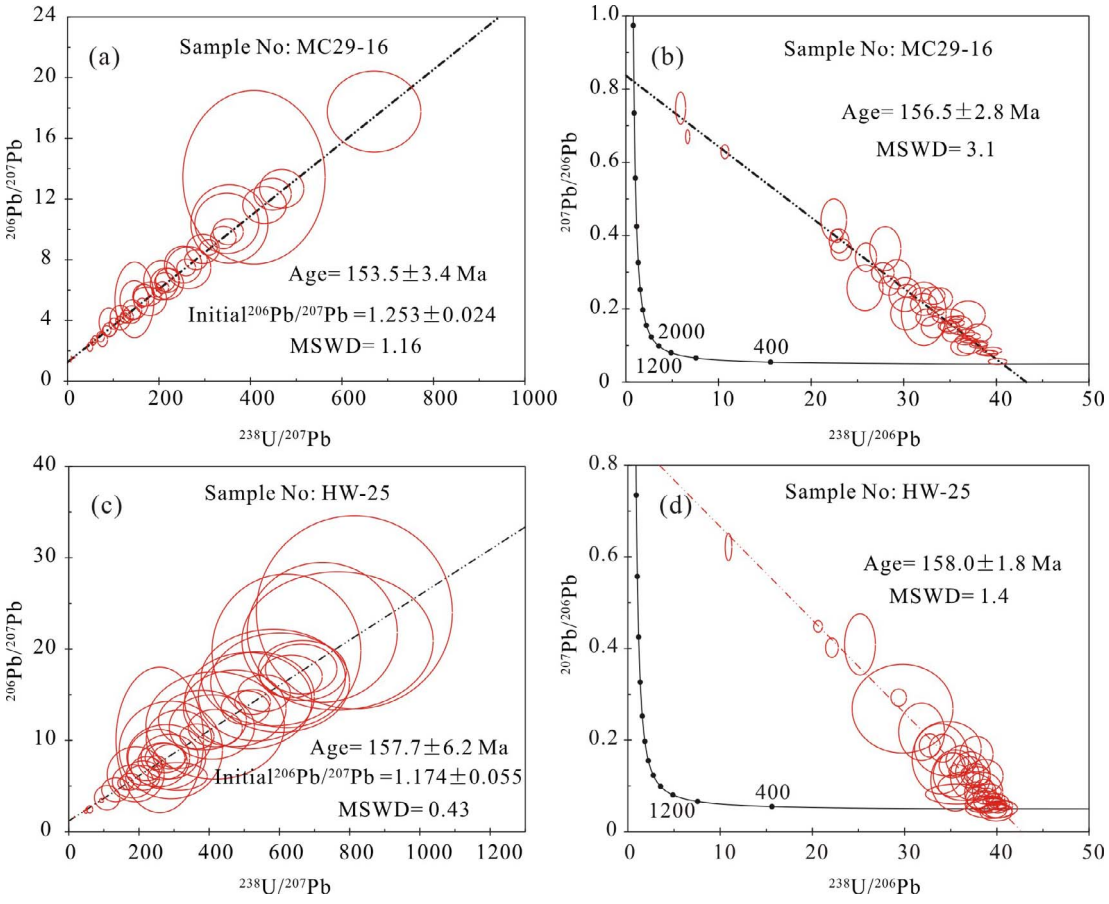

Fig. 7. $^{206}Pb/^{207}Pb$ versus $^{238}U/^{207}Pb$ "isochron" and Tera–Wasserburg diagrams for cassiterite from the Maozaishan Sn deposit. (a, b) "isochron" and Tera-Wasserburg diagrams, respectively, for sample MC29-16; (c, d) "isochron" and Tera-Wasserburg diagrams, respectively, for sample HW-25.

values from other W and Sn deposits along this belt, such as the Shizhuyuan W-dominated polymetallic deposit and the Xianghualing and Furong Sn deposits (Figs. 10 and 11). These data indicate that mixed crustal sources played important roles during ore formation in the Qin-Hang belt (Fig. 11), an interpretation supported by the trace element geochemistry and isotopic data (Sr, Nd, Pb, Hf and He-Ar) for the Guposhan Sn orefield and the Xianghualing, Furong and Hehuaping Sn deposits (Fig. 1b) (Chen et al., 2014; Hu et al., 2012; Li et al., 2006; Liang et al., 2016; Shan et al., 2014; Wu et al., 2011). Thus, the various lines of geological and isotopic evidence show that crust-mantle interaction was involved in Sn mineralization in the Dayishan orefield, which may imply a special geodynamic environment.

6.3. Geodynamic setting of metallogeny

The Nanling Range is rich in W-Sn resources (Lehmann, 1990) and there are numerous large W and Sn deposits in the region (Huang et al., 2003). Previous studies have suggested that the nature of the mineralization in the region changed from east to west, with dense W mineralization predominantly in the east and Sn mineralization increasing westward (Hua et al., 2010). Most Sn deposits in this range are clustered in, or close to, the NE-trending Qin-Hang belt, which is located along the Neoproterozoic suture between the Yangtze and Cathaysia Blocks that was reactivated during the Late Jurassic (Mao et al., 2011). Accompanying these geological events there were many types of mineralization, such as the Neoproterozoic volcanic-hosted, massive sulfide, Cu-dominated polymetallic deposits, exhalative Pb-Zn-Ag-polymetallic deposits (Zhou et al., 2017) and W-Sn-Cu-Pb-Zn deposits related to the Yanshanian granitoids (Guo et al., 2013). The granitoid-related W-Sn deposits are mostly concentrated in the Nanling Range and mostly formed during the Late Jurassic (Mao et al., 2011). The granitoids associated with these deposits are commonly rich in MMEs and display mantle signatures, such as high Nd(t) and εHf values with young two-stage model ages (Gilder et al., 1996; Hua et al., 2010). These granites display typical A_2-type characteristics such as elevated Zr + Nb + Ce + Y (> 340 ppm) and REE contents, flat REE patterns and high 10,000*Ga/Al ratios (> 2.6) (Huang et al., 2011; Li et al., 2014; Zhao et al., 2005; Zhou et al., 2013). On the basis of the mantle

Table 3
Molybdenite Re–Os isotope composition for molybdenite–quartz vein.

Sample	Weight (g)	Re (ng/g)	2σ	C_{Os} (ng/g)	2σ	^{187}Re (ng/g)	2σ	^{187}Os (ng/g)	2σ	Age (Ma)	2σ
PD2-06	0.02531	94.94	0.28	0.8080	0.0027	59.67	0.17	0.168	0.0005	168.8	0.8
PD2-08	0.04907	5570	16	0.3544	0.0013	3501	10	8.977	0.0290	153.7	0.7
PD2-09	0.10044	4049	13	0.1574	0.0006	2545	8	6.854	0.0240	161.4	0.8
PD2-09	0.05042	4153	33	0.0578	0.0081	2610	21	7.089	0.0510	162.8	2.4
PD2-10	0.05228	4316	32	0.0238	0.0092	2713	20	7.390	0.0470	163.3	2.3

C_{os}: Common Os.

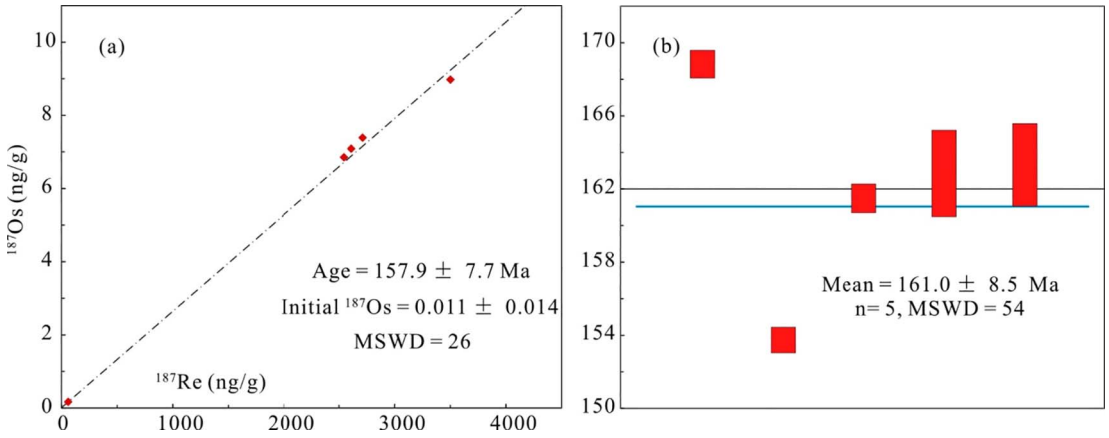

Fig. 8. Result of molybdenite Re–Os dating. (a) isochron model age; and (b) weighted age for quartz–molybdenite vein from the Maozaishan Sn deposit.

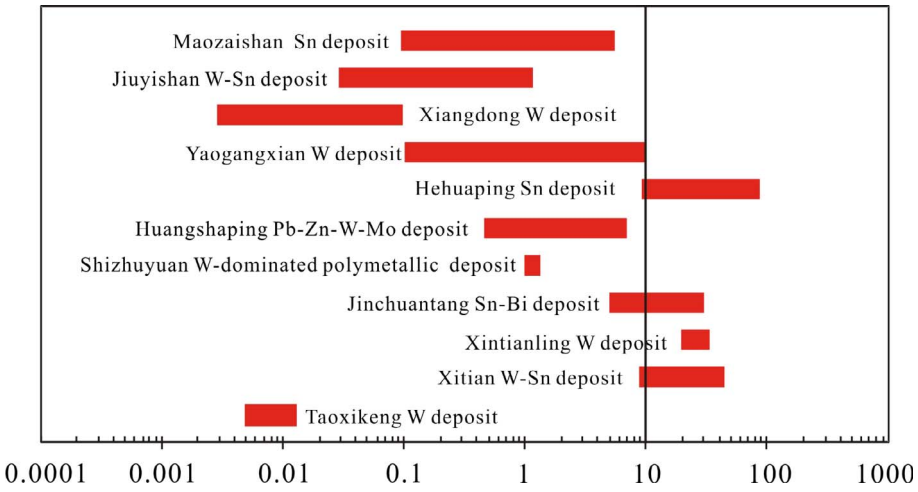

Fig. 9. Molybdenite Re contents of Sn, W and W–Sn deposits in the Nanling Range. These data were collected from the Taoxikeng W deposit (Guo et al., 2011), Xitian W–Sn deposit (Liang et al., 2016), Xintianling W deposit (Yuan et al., 2012), Jinchuantang Sn–Bi deposit (Liu et al., 2012), Shizhuyuan W-dominated, polymetallic deposit (Li and Sun, 2012), Huangshaping Pb–Zn–W–Mo deposit (Yao et al., 2007), Hehuaping Sn deposit (Cai et al., 2006), Yaogangxian W deposit (Li et al., 2011), Xiangdong W deposit (Cai et al., 2012) and Jiuyishan W–Sn deposit (Fu et al., 2007). The red boxes represent the range of data from each site.

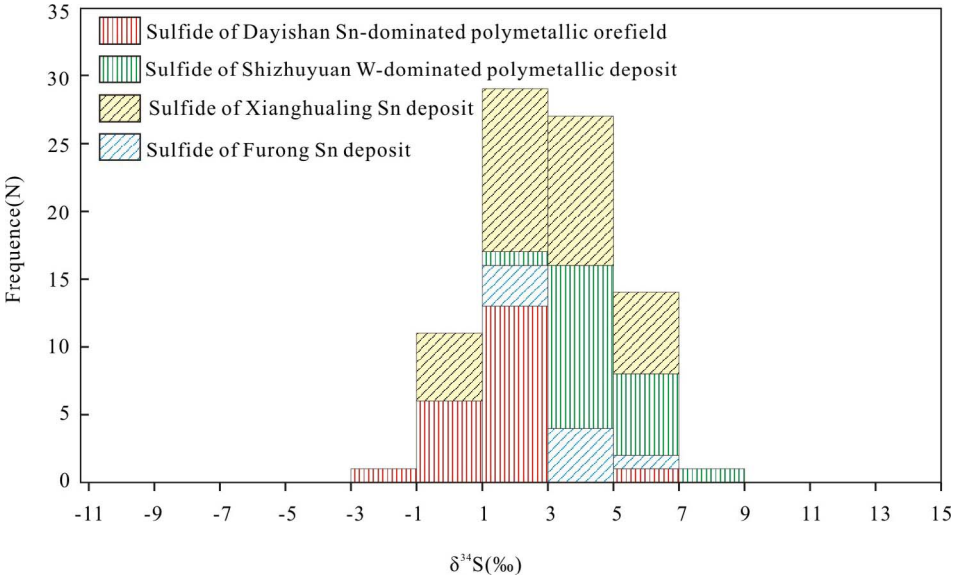

Fig. 10. Histogram of δ^{34}S values for the Dayishan Sn orefield and the Furong Sn deposit in the Nanling Range. These isotopic data were collected from the Dayishan Sn-dominated polymetallic orefield (Zeng, 2013), Furong Sn deposit (Li, 2006), Shizhuyuan W-dominated polymetallic deposit (Liu et al., 2006) and Xianghualing Sn deposit (Zhou et al., 2008).

signatures discussed above, it is likely that the magmatism and hydrothermal activity in this region was associated with lithospheric thinning and crustal extension (Gilder et al., 1996; Li et al., 2006, 2009b; Zhao et al., 2012). For example, Mao et al. (2007, 2008) and Wang et al. (2014) have suggested that large-scale W-Sn mineralization at 160–150 Ma in this area developed as a result of a slab window or slab break-off.

As mentioned in Section 2, the Dayishan orefield is part of the NE-

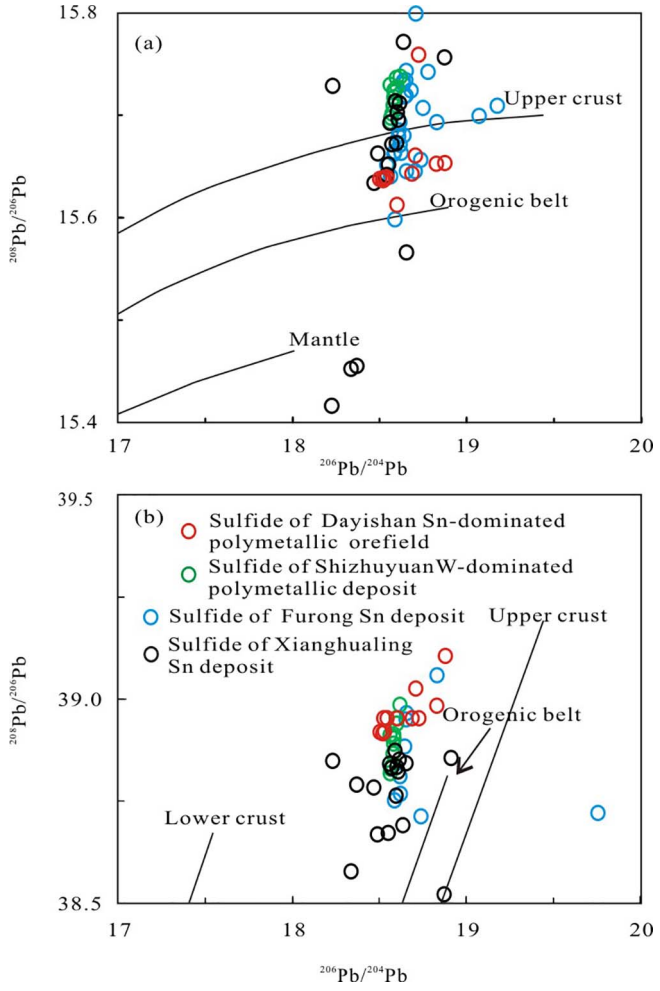

Fig. 11. (a) $^{206}Pb/^{204}Pb$ vs. $^{207}Pb/^{204}Pb$ and (b) $^{206}Pb/^{204}Pb$ vs. $^{208}Pb/^{204}Pb$ plots of sulfide samples from the Dayishan Sn-dominated polymetallic orefield (Zeng, 2013), Furong Sn deposit (Li, 2006), Shizhuyuan W–dominated polymetallic deposit (Wu et al., 2016) and Xianghualing Sn deposit (Zhou et al., 2008). The tectonic-geologic discrimination fields are modified after Zartman and Doe (1981).

trending Qin-Hang belt, located at the intersection of the Youxian-Ningyuan (NE-trending), Shaoyang-Chenzhou (NW-trending) and Yangmingshan-Tashan-Shangbao (E-W-trending) fault belts. These faults and older, long-lived, E-W-trending faults, were sites of concentrated magmatism and mineralization. Isotopic data from ore minerals of the Maozaishan deposit show distinct mixed signatures and the granite that is genetically related to the Sn mineralization has A_2-type geochemical characteristics (Kong et al., 2014; Zhang et al., 2014). There is also evidence of high-temperature granites with no inherited zircons. Previous studies have shown that the Paleo-Pacific Plate subducted beneath the Eurasian continent from 160 to 150 Ma, resulting in the formation of a number of parallel, NE-trending, extensional belts along the Qin–Hang zone in a back–arc region where mantle-crust interaction was strong (Mao et al., 2007; Peng et al., 2006). Thus, we infer that the Dayishan orefield, located at the intersection of major faults within the Qin-Hang belt, was formed from A-type granitic magmas produced by mixing of crustal and mantle melts.

7. Conclusions

The mineralization age of the Maozaishan Sn deposit, which represents a typical Sn deposit in the Dayishan orefield, is constrained by geochronological examination of molybdenite separates from molybdenite-quartz veins, zircon grains from unaltered, ore-related, porphyry monzogranite and cassiterite separates from both altered granite and greisen-quartz vein-type mineralization.

The cassiterite U-Pb concordia age of ca. 158–156 Ma represents the age of Sn mineralization in this area, which is, within analytical error, the same as the molybdenite Re-Os and zircon U-Pb ages. This strongly suggests a genetic link between the Sn mineralization and granitic magmatism.

Isotopic data also confirm that the Sn deposits in the Dayishan orefield contain mixed sources similar to other W and Sn deposits in the Nanling Range. The formation of the Sn deposits in this region was most likely associated with lithospheric thinning and crustal extension along the Qin-Hang belt during the Late Jurassic.

Acknowledgments

We thank Pro. Hongying Zhou of the Tianjin Institute of Geology and Mineral Resources, Prof. Chao Li of the National Research Center of Geoanalysis, and Prof. Kuidong Zhao of the China University of Geosciences (Wuhan) for their helpful instructions and discussions during the cassiterite, molybdenite and zircon analyses. Comments by Prof. Meifu Zhou and two anonymous reviewers have been important in improving the final presentation of this work. This study was supported by grants from the National Key Research and Development Program (No. 2016YFC0600208), “Fundamental Research Funds for the Central Universities” (No. 310827171122), and Geological Survey Projectof China Geological Survey project (No. DD20170050).

References

Cai, M.H., Chen, K.X., Qu, W.J., Liu, G.Q., Fu, J.M., Yin, J.P., 2006. Geological characteristics and Re–Os dating of molybdenites in Hehuaping tin–polymetallic deposit, southern Hunan Province. Miner. Deposita 25 (3), 263–268 (in Chinese with English abstract).

Cai, Y., Ma, D.S., Lu, J.J., Huang, B., Zhang, R.Q., Qu, W.J., 2012. Re–Os geochronology and S isotope geochemistry of Dengfuxian tungstern deposit, Hunan Province. Acta Petrol. Sin. 28 (12), 3798–3808 (in Chinese with English abstract).

Chen, J., Wang, R.C., Zhu, J.C., Lu, J.J., Ma, D.S., 2014. Multiple–aged granitoids and related W-Sn mineralization in the Nanling Range, South China. Sci. China, Ser. D Earth Sci. 56, 2045–2055.

Deng, X.H., Chen, Y.J., Bagas, L., Zhou, H.Y., Zheng, Z., Yue, S.W., Chen, H.J., Li, H.M., Tu, J.R., Cui, Y.R., 2017. Cassiterite U-Pb geochronology of the Kekekaerde W-Sn deposit in the Baiganhu ore field, East Kunlun Orogen, NW China: timing and tectonic setting of mineralization. Ore Geol. Rev. http://dx.doi.org/10.1016/j.oregeorev.2017.02.018. in press.

Du, A.D., Wu, S., Sun, D., Wang, S., Qu, W., Markey, R., Stain, H., Morgan, J., Malinovskiy, D., 2004. Preparation and certification of Re–Os dating reference materials: molybdenites HLP and JDC. Geostand. Geoanal. Res. 28 (1), 41–52.

Fu, J.M., Li, H.Q., Qu, W.J., Yang, X.J., Wei, J.Q., Liu, G.Q., Ma, L.Y., 2007. Re–Os isotope dating of the Da'ao tungsten–tin deposit in the Jiuyi Mountains, southern Hunan Province. Geol. China 34 (4), 651–656 (in Chinese with English abstract).

Gilder, S.A., Gill, J., Coe, R.S., Zhao, X., Liu, Z., Wang, G., Yuan, K., Liu, W., Kuang, G., Wu, H., 1996. Isotopic and paleomagnetic constraints on the Mesozoic tectonic evolution of south China. J. Geophys. Res. Solid Earth 101, 16137–16154.

Guo, C., Mao, J., Bierlein, F., Chen, Z., Chen, Y., Li, C., Zeng, Z., 2011. SHRIMP U-Pb (zircon), Ar–Ar (muscovite) and Re–Os (molybdenite) isotopic dating of the Taoxikeng tungsten deposit, South China Block. Ore Geol. Rev. 43 (1), 26–39.

Guo, C.L., Xu, Y.M., Lou, F.S., Zzheng, J.H., 2013. A comparative study of the Middle Jurassic granodorite related to Cu and the Late Jurassic granites related to Sn in the Qin-Hang metallogenic belt and a tentative discussion on their tectonic dynamic setting. Acta Petrol. Mineral. 32 (4), 463–484 (in Chinese with English Abstract).

Hsieh, P.S., Chen, C.H., Yang, H.J., Lee, C.Y., 2008. Petrogenesis of the Nanling mountains granites from South China: constraints from systematic apatite geochemistry and whole–rock geochemical and Sr–Nd isotope compositions. J. Asian Earth Sci. 33 (5–6), 428–451.

Hu, R.Z., Bi, X.W., Jiang, G.H., Chen, H.W., Peng, J.T., Qi, Y.Q., Wu, L.Y., Wei, W.F., 2012. Mantle–derived noble gases in ore–forming fluids of the granite-related Yaogangxian tungsten deposit, Southeastern China. Miner. Deposita 47 (6), 623–632.

Hu, R.Z., Chen, W.T., Xu, D.R., Zhou, M.F., 2017. Reviews and new metallogenic models of mineral deposits in South China: an introduction. J. Asian Earth Sci. 137, 1–8.

Hua, R.M., Li, G.L., Zhang, W.L., Hu, D.L., Chen, P.R., Chen, W.F., Wang, X.D., 2010. A tentative discussion on differences between large-scale tungsten and tin mineralizations in South China. Miner. Deposita 29 (1), 9–23.

Huang, G.F., Gong, S.Q., Jiang, X.W., Tan, S.X., Li, C.B., Liu, D.H., 2003. Exploration on the ore–forming regularities of the tin deposits in Qitianling area, southern Hunan. Geol. Bull. China 22, 445–451 (in Chinese with English abstract).

Huang, H.Q., Li, X.H., Li, W.X., Li, Z.X., 2011. Formation of high ^{18}O fayalite-bearing A-type granite by high-temperature melting of granulitic metasedimentary rocks,

southern China. Geology 39, 903–906.
Ji, W.B., Lin, W., Faure, M., Chen, Y., Chu, Y., Xue, Z.H., 2017. Origin of the Late Jurassic to Early Cretaceous peraluminous granitoids in the northeastern Hunan province (middle Yangtze region), South China: geodynamic implications for the Paleo-Pacific subduction. J. Asian Earth Sci. 141, 174–193.
Kong, H., Fei, L.D., Jiang, L.Z., Wang, G., Liu, S.J., Zhou, W.P., Quan, T.J., 2014. Zircon U-Pb ages and Hf isotope and their geological significance of granites in Xinsheng deposit, Hunan Province, China. Trans. Nonferrous Met. Soc. 178 (24), 229–238 (in Chinese with English abstract).
Lehmann, P.D.B., 1982. Metallogeny of tin; magmatic differentiation versus geochemical heritage. Econ. Geol. 77 (1), 50–59.
Lehmann, P.D.B., 1990. Metallogeny of Tin. Lecture Notes in Earth Sciences 32 Springer Verlag, Berlin pp. 1–177.
Li, Z.L., 2006. Geochemical relationship between tin mineralization and A–type granite: a case of the Furogn tin ore field, Hunan Province, South China. Doctoral dissertation. Institute of Geochemistry, Chinese Academy of Sciences (in Chinese with English abstract).
Li, H.Y., Sun, Y.L., 2012. Re–Os isotopic chronology of molybdenite in the Shizhuyuan polymetallic tungsten deposit, South Hunan. Geol. Rev. 42 (3), 261–267 (in Chinese with English abstract).
Li, Z.L., Peng, J.T., Bi, X.W., Li, X.M., 2006. Helium isotope composition of fluid inclusions and the origin of ore–Forming fluids of the Furong tin orefield in Hunan Province, China. Earth Sci. 31 (1), 129–135 (in Chinese with English abstract).
Li, X.H., Li, W.X., Li, Z.X., Lo, C.H., Wang, J., Ye, M.F., Yang, Y.H., 2009a. Amalgamation between the Yangtze and Cathaysia Blocks in South China: constraints from SHRIMP U-Pb zircon ages, geochemistry and Nd–Hf isotopes of the Shuangxiwu volcanic rocks. Precambr. Res. 174 (1), 117–128.
Li, X.H., Li, W.X., Wang, X.C., Li, Q.L., Yu, L., Tang, G.Q., 2009b. Role of mantle–derived magma in genesis of early Yanshanian granites in the Nanling Range, South China: in situ zircon Hf–O isotopic constraints. Sci. China, Ser. D Earth Sci. 52 (9), 1262–1278.
Li, S.T., Wang, J.B., Zhu, X.Y., Li, C., 2011. Re–Os dating of molybdenite and sulfur isotope analysis of the Yaogangxian tungsten polymetallic deposits in Hunan Province and their geological significance. Geoscience 25 (2), 228–235 (in Chinese with English abstract).
Li, H., Watanabe, K., Yonezu, K., 2014. Geochemistry of A–type granites in the Huangshaping polymetallic deposit (South Hunan, China): implications for granite evolution and associated mineralization. J. Asian Earth Sci. 88 (4), 149–167.
Li, C.Y., Zhang, R.Q., Ding, X., Ling, M.X., Fan, W.M., Sun, W.D., 2016. Dating cassiterite using laser ablation ICP–MS. Ore Geol. Rev. 72 (Part 1), 313–322.
Liang, X.Q., Dong, C.G., Jiang, Y., Wu, S.C., Zhou, Y., Zhu, H.F., Fu, J.G., Wang, C., Shan, Y.H., 2016. Zircon U-Pb, molybdenite Re–Os and muscovite Ar–Ar isotopic dating of the Xitian W–Sn polymetallic deposit, eastern Hunan Province, South China and its geological significance. Ore Geol. Rev. 78, 85–100.
Liu, Y.R., Kuang, J., Ma, T.Q., Bai, D.Y., 2006. ^{40}Ar–^{39}Ar dating of biotite in south Dayishan granite and its geological significance. Resour. Surv. Environ. 26 (4), 244–249 (in Chinese with English abstract).
Liu, Y., Hu, Z., Zong, K., Gao, C., Gao, S., Xu, J., Chen, H., 2010a. Reappraisal and refinement of zircon U-Pb isotope and trace element analyses by LA–ICP–MS. Chin. Sci. Bull. 55 (15), 1535–1546 (in Chinese with English abstract).
Liu, Y., Gao, S., Hu, Z., Gao, C., Zong, K., Wang, D., 2010b. Continental and oceanic crust recycling-induced melt-peridotite interactions in the Trans-North China Orogen: U-Pb dating, Hf isotopes and trace elements in zircons from mantle xenoliths. J. Petrol. 51 (51), 392–399.
Liu, X.F., Yuan, S.D., Shenghua, A.W., 2012. Re–Os dating of the molybdenite from the Jinchuantang tin–bismuth deposit in Hunan Province and its geological significance. Acta Petrol. Sin. 28 (1), 39–51 (in Chinese with English abstract).
Liu, P., Mao, J.W., Cheng, Y.B., Yao, W., Wang, X.Y., Hao, D., 2017. An early Cretaceous W-Sn deposit and its implications in southeast coastal metallogenic belt: constraints from U-Pb, Re-Os, Ar-Ar geochronology at the Feie'shan W-Sn deposit, SE China. Ore Geol. Rev. 81, 112–122.
Mao, J.W., Zhang, Z.C., Zhang, Z.H., Du, A.D., 1999. Re–Os isotopic dating of molybdenites in the Xiaoliugou W (Mo) deposit in the northern Qilian Mountains and its geological significance. Geochim. Cosmochim. Acta 63 (11–12), 1815–1818 (in Chinese with English abstract).
Mao, J.W., Xie, G.Q., Guo, C.L., Chen, Y.C., 2007. Large–scale tungsten–tin mineralization in the Nanling region, South China: metallogenic ages and corresponding geodynamic processes. Acta Petrol. Sin. 23 (10), 2329–2338 (in Chinese with English abstract).
Mao, J.W., Chen, M.H., Yuan, S.D., Guo, C.L., 2011. Geological characteristics of the Qinhang(or Shihang) Metallogenic Belt in South China and spatial–temporal distribution regularity of mineral deposits. Acta Geol. Sin. 85 (5), 636–658 (in Chinese with English abstract).
Peng, J.T., Zhou, M.F., Hu, R., Shen, N., Yuan, S., Bi, X., Du, A., Qu, W., 2006. Precise molybdenite Re–Os and mica Ar–Ar dating of the Mesozoic Yaogangxian tungsten deposit, central Nanling district, South China. Miner. Deposita 41 (7), 661–669 (in Chinese with English abstract).
Peng, J.T., Hu, R.Z., Yuan, S.D., Bi, X.W., Shen, N.P., 2008. The time ranges of granitoid emplacement and related nonferrous metallic mineralization in southern Hunan. Geol. Rev. 54 (5), 617–625 (in Chinese with English abstract).
Shan, Q., Zeng, Q.S., Li, J.K., Lu, H.Z., Hou, M.Z., Yu, X.Y., Wu, C.J., 2014. Diagenetic and metallogenic source of the Furong tin deposit, Qitianling: constraints from Lu–Hf for zircon and He–Ar isotopes of fluid inclusions. Acta Geol. Sin. 88 (4), 704–715 (in Chinese with English abstract).
Shirey, S.B., Walker, R.J., 1995. Carius tube digestion for low–blank Rhenium-Osmium analysis. Anal. Chem. 67 (13), 2136–2141.
Smoliar, M.I., Walker, R.J., Morgan, J.W., 1996. Re–Os ages of group IIA, IIIA, IVA, and IVB iron meteorites. Science 271, 1099–1102.
Wang, D.Z., Shu, L.S., 2012. Late Mesozoic basin and range tectonics and related magmatism in Southeast China. Geosci. Front. 3, 109–124.
Wang, Y.L., Peng, Q.M., Zhu, X.Y., Cheng, X.Y., Li, S.T., 2014. Geochemical and chronological characteristics of the granite porphyry in the Jiepailing tin–polymetallic deposit, Hunan Province and mineralization belt division. Geol. Explor. 50 (3), 475–485 (in Chinese with English abstract).
Wu, G.Y., Peng, H., 2000. Geological features and emplacement mechanism of the Dayishan granitic intrusion in south Hunan Province. Geol. Miner. Resour. South China 3, 1–7 (in Chinese with English abstract).
Wu, G.Y., Pan, Z.F., Hou, Z.Q., Li, J.D., Che, L.I., Chen, Q.J.H.M., 2005. Ore body distribution pattern, ore-controlling factors and prospecting potentiality in the Dayishan tin deposit, Hunan Province. Geol. Prospect. 41 (2), 6–11 (in Chinese with English abstract).
Wu, Y.C., Zheng, B.R., Tang, Z.H., 2008. Characteristics and ore prospecting of tin deposits in the Dayishan area, Hunan Province. Geol. Prospect. 44 (4), 14–19 (in Chinese with English abstract).
Wu, L.Y., Hu, R., Peng, J.T., Bi, X.W., Jiang, G.H., Chen, H.W., Wang, Q.Y., Liu, Y.Y., 2011. He and Ar isotopic compositions and genetic implications for the giant Shizhuyuan W–Sn–Bi–Mo deposit, Hunan Province, South China. Int. Geol. Rev. 53 (5–6), 677–690.
Wu, S.H., Dai, P., Wang, X.D., 2016. C, H, O and Pb isotopic geochemistry of W–polymetallic skarn–greisen and Pb–Zn–Ag veins in the Shizhuyuan ore field, Hunan Province. Miner. Deposita 35 (3), 633–647.
Yan, Q.H., Qiu, Z.W., Wang, H., Wang, M., Wei, X.P., Li, P., Zhang, R.Q., Li, C.Y., Liu, J.P., 2016. Age of the Dahongliutan rare metal pegmatite deposit, West Kunlun, Xinjiang (NW China): constraints from LA–ICP–MS U-Pb dating of columbite–(Fe) and cassiterite. Ore Geol. Rev. http://dx.doi.org/10.1016/j.oregeorev.2016.11.010.
Yao, J.M., Hua, R.M., Qu, W.J., Qi, H.W., Lin, J.F., Du, A.D., 2007. Re–Os isotope dating of molybdenites in the Huang shaping Pb–Zn–W–Mo polymetallic deposit, Hunan Province, South China and its geological significance. Sci. China, Ser. D Earth Sci. 50 (4), 519–526 (in Chinese with English abstract).
Yu, J.H., Zhou, X., O'Reilly, S.Y., Zhao, L., Griffin, W.L., Wang, R., Wang, L., Chen, X., 2005. Formation history and protolith characteristics of granulite facies metamorphic rock in central Cathaysia deduced from U-Pb and Lu–Hf isotopic studies of single zircon grains. Chin. Sci. Bull. 50 (18), 2080–2089.
Yuan, S., Peng, J., Hu, R., Li, H., Shen, N., Zhang, D., 2008. A precise U-Pb age on cassiterite from the Xianghualing tin–polymetallic deposit (Hunan, South China). Miner. Deposita 43 (4), 375–382.
Yuan, S., Peng, J., Hao, S., Li, H., Geng, J., Zhang, D., 2011. In situ LA–MC–ICP–MS and ID–TIMS U-Pb geochronology of cassiterite in the giant Furong tin deposit, Hunan Province, South China: new constraints on the timing of tin–polymetallic mineralization. Ore Geol. Rev. 43, 235–242.
Yuan, S.D., Zhang, D.L., Shuang, Y., Du, A.D., Qu, W.J., 2012. Re–Os dating of molybdenite from the Xintianling giant tungsten–molybdenum deposit in southern Hunan province, China and its geological implications. Acta Petrol. Sin. 28 (1), 27–38 (in Chinese with English abstract).
Yuan, S.D., Mao, J.W., Nigel, J.C., Wang, X.D., Liu, X.F., Yuan, Y.B., 2015. A Late Cretaceous tin metallogenic event in Nanling W-Sn metallogenic province: constraints from U-Pb, Ar-Ar geochronology at the Jiepailing Sn-Be-F deposit, Hunan, China. Ore Geol. Rev. 65, 283–293.
Zartman, R.E., Doe, B.R., 1981. Plumbotectonics–the model. Tectonophysics 75, 135–162.
Zeng, Z.F., 2013. Study on the Structure and Metallogenic Mechanism of Dayishan tin Deposit, Hunan Province. China University of Geosciences, Beijing (in Chinese with English abstract).
Zhang, X.J., Luo, H., Wu, Z.H., Fan, X.W., Xiong, J., Yang, J., Mou, J.Y., 2014. Rb–Sr isochron age and its geological significance of Baishaziling tin deposit in Dayishan ore field, Hunan Province. Earth Sci. 39 (10), 1322–1332 (in Chinese with English abstract).
Zhang, R.Q., Lu, J.J., Wang, R.C., Yang, P., Zhu, J.C., Yao, Y., Gao, J.F., Li, C., Lei, Z.H., Zhang, W.L., Guo, W.M., 2015. Constraints of in situ zircon and cassiterite U-Pb, molybdenite Re–Os and muscovite ^{40}Ar–^{39}Ar ages on multiple generations of granitic magmatism and related W-Sn mineralization in the Wangxianling area, Nanling Range, South China. Ore Geol. Rev. 65 (4), 1021–1042.
Zhao, K.D., Jiang, S.Y., Jiang, Y.H., Wang, R.C., 2005. Mineral chemistry of the Qitianling granitoid and the Furong tin ore deposit in Hunan Province, South China: implication for the genesis of granite and related tin mineralization. Eur. J. Mineral. 17 (4), 635–648.
Zhao, J.H., Zhou, M.F., Yan, D.P., Zheng, J.P., Li, J.W., 2011. Reappraisal of the ages of Neoproterozoic strata in South China: no connection with the Grenvillian orogeny. Geology 39, 299–302.
Zhao, K.D., Jiang, S.Y., Yang, S.Y., Dai, B.Z., Lu, J.J., 2012. Mineral chemistry, trace elements and Sr–Nd–Hf isotope geochemistry and petrogenesis of Cailing and Furong granites and mafic enclaves from the Qitianling batholith in the Shi-Hang zone, South China. Gondwana Res. 22 (1), 310–324.
Zhao, W.W., Zhou, M.F., Li, Y.H.M., Zhao, Z., Gao, J.F., 2017. Genetic types, mineralization styles, and geodynamic settings of Mesozoic tungsten deposits in South China. J. Asian Earth Sci. 137, 109–140.
Zhao, Z., Zhao, W.W., Lu, L., Wang, H.Y., 2018. Constraints of multiple dating of the Qingshan tungsten deposit on the Triassic W(-Sn) mineralization in the Nanling region, South China. Ore Geol. Rev. http://dx.doi.org/10.1016/j.oregeorev.2018.01.009.
Zhou, H.X., Yang, G.H., Jiang, Z.H., Chen, Q.C., 2005. Geological characteristics and origin of the Dayishan tin orefield in the Nanling region. Geol. Miner. Resour. South China 2, 87–94 (in Chinese with English abstract).
Zhou, T., Liu, W.H., Li, H., Xu, W.X., Dai, T.G., 2008. Isotope geochemistry of the

Xianghualing tin–polymetallic deposit in Hunan Province. Acta Geosci. Sin. 29 (6), 703–708.
Zhou, Y., Liang, X., Wu, S., Jiang, Y., Wen, S., Cai, Y., 2013. Geochronology and geochemical characteristics of the Xitian tungsten–tin-bearing A-type granites, Hunan Province, China. Geotect. Metall. 37 (3), 511–529.
Zhou, M.-F., Zhao, X.F., Chen, W.T., Li, X.C., Wang, W., Yan, D.P., Qiu, H.N., 2014. Proterozoic Fe–Cu metallogeny and supercontinental cycles of the southwestern Yangtze Block, southern China and northern Vietnam. Earth Sci. Rev. 139, 59–82.
Zhou, Y.Z., Li, X.Y., Zheng, Y., Shen, W.J., He, J.G., Yu, P.P., Niu, J., Zeng, C.Y., 2017. Geological settings and metallogenesis of Qinzhou Bay-Hangzhou Bay orogenic juncture belt, South China. Acta Petrol. Sin. 33 (3), 667–681.
Zhu, J.C., Chen, J., Wang, R.C., Lu, J.J., Xie, L., 2008. Early Yanshanian NE-trending Sn/W-bearing A-type granites in the western-middle part of the Nanling Mts region. Geol. J. China Univ. 14 (4), 474–484 (in Chinese with English abstract).